AIAA JOURNAL
Vol. 43, No. 4, April 2005

Unsteady Calibration of Fast-Response Pressure Probes, Part 1: Theoretical Studies

Espen S. Johansen* and Othon K. Rediniotis†
Texas A&M University, College Station, Texas 77843-3141

Recent advances in miniaturization of pressure transducers, including microelectromechanical systems technology, have provided miniature, high-bandwidth pressure transducers and transducer arrays well suited for fast-response, multihole probes. The miniature size of these arrays enables a design in which the transducers are embedded in, or close to, the probe tip while maintaining a tip diameter of 1–2 mm. Although the frequency response of such a probe is excellent, there are several unresolved issues pertaining to fluid inertia-related unsteady aerodynamic effects on probe calibration. As a result of these effects, when the probe is used in a dynamically changing flowfield a quasi-steady probe calibration can no longer be used to resolve the instantaneous velocity vector. We present theoretical analysis of these effects and formulate methods of calibrating multihole, fast-response probes for use in unsteady flows in order to accurately resolve the instantaneous velocity vector. The main objective of the theoretical analysis is to study and quantify the dependence of the probe measured pressures on the magnitude of the flow inertial effects in terms of properly formulated nondimensional parameters, as well as allow a direct comparison of theory and experiment. Among the contributions of this work, it was particularly interesting to find that proper definition of the nondimensional, flow-angle-dependent pressure coefficients renders them insensitive to unsteady effects. This has the significant ramification that the steady calibration of these coefficients can be also used in unsteady flowfields for the calculation of the flow angles. Calculation of the velocity magnitude, however, requires quantification of and correction for the fluid inertial effects.

Nomenclature

B_α	=	pressure coefficient (low angle)
B_β	=	pressure coefficient (low angle)
Cp	=	pressure coefficient
Cp_S	=	steady pressure coefficient
Cp_{STEADY}	=	steady pressure coefficient
Cp_U	=	unsteady pressure coefficient
Cp_{UNSTEADY}	=	unsteady pressure coefficient
K	=	nondimensional acceleration
K_{MAX}	=	maximum value of K
K_{RMS}	=	rms value of K
p	=	pressure, Pa
p_s	=	static pressure, Pa
p_t	=	total pressure, Pa
q_{dyn}	=	dynamic pressure, Pa
R	=	probe tip radius, m
r	=	r coordinate, m (spherical coordinate system)
$\hat{r}$	=	unit vector in r direction
t	=	time, s
$U(t)$	=	instantaneous velocity, m/s
$\bar{U}$	=	mean velocity, m/s
α	=	pitch angle, deg
β	=	yaw angle, deg
Δp	=	$p - p_s$, Pa
θ	=	cone angle and θ coordinate, deg
$\hat{\theta}$	=	unit vector in θ direction
λ	=	wavelength, m
ρ	=	density, kg/m^3
Φ	=	velocity potential, m^2/s
ϕ	=	roll angle, deg
ω	=	frequency, rad/s
ω^*	=	nondimensional frequency

Received 6 June 2002; accepted for publication 7 July 2004. Copyright © 2004 by Espen S. Johansen and Othon K. Rediniotis. Published by the American Institute of Aeronautics and Astronautics, Inc., with permission. Copies of this paper may be made for personal or internal use, on condition that the copier pay the $10.00 per-copy fee to the Copyright Clearance Center, Inc., 222 Rosewood Drive, Danvers, MA 01923; include the code 0001-1452/05 $10.00 in correspondence with the CCC.

*Postdoctoral Research Associate, Department of Aerospace Engineering. Member AIAA.
†Associate Professor, Department of Aerospace Engineering. Associate Fellow AIAA.

Introduction

THE multihole pressure probe is a proven and mature measurement technology to resolve the three-dimensional velocity vector in steady flowfields.[1–4] In unsteady flowfields, however, other instruments, such as the hot-wire anemometer, have typically been preferred. This is because of several unresolved issues related to pressure probes, such as miniaturization, frequency response, and unsteady aerodynamic and acoustic effects. The significant challenges (and associated expense) in resolving the instantaneous three-dimensional velocity field with commercially available instrumentation, such as hot-wire, laser Doppler velocimetry, particle image velocimetry, or Doppler global velocimetry have instigated efforts to resolve the pressure-probe-related issues and develop miniature, fast-response, multihole probes.

A number of researchers have designed fast-response, multihole probes to resolve unsteady flowfields.[5–16] Kerrebrock et al.[7] designed a probe with high-frequency response (30 kHz), but with a large probe tip diameter (5 mm). Ng and Popernack[9] developed a four-sensor probe with a diameter of 5.2 mm and a frequency response of 20 kHz. Matsunaga et al.[8] developed a probe with small tip diameter (2 mm), but with a limited frequency response (500 Hz). Naughton et al.[10,11] developed a five-hole probe for supersonic flow measurements with a 1.1-mm probe tip, but frequency response limited to 50 Hz. In most of these efforts, the frequency response limitations were caused by the tubing leading from the probe tip to the pressure transducers mounted in the probe body.

In recent years, significant progress has been made in the miniaturization of pressure transducers. Using microelectromechanical systems (MEMS) technology, pressure transducers with a length scale of 0.1 mm and frequency response of 100 kHz have become available.[17,18] These transducers can be incorporated at or near the probe tip, thus decreasing or altogether eliminating tubing. Very short pressure transmission paths from the probe tip to the transducer diaphragm allow for high bandwidth without associated attenuation and phase lag in the measured pressure. The miniature size of the transducer or transducer array enables the design of five- or

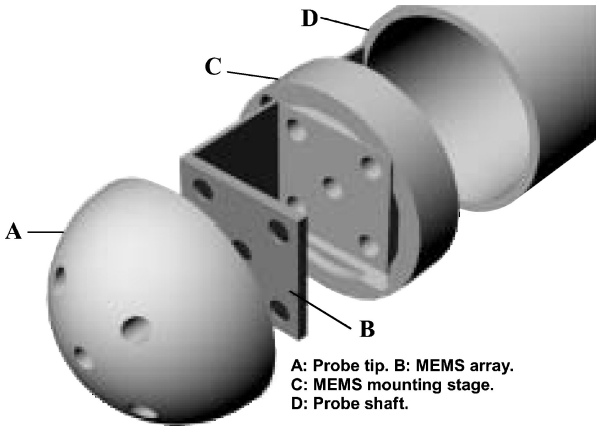

a)

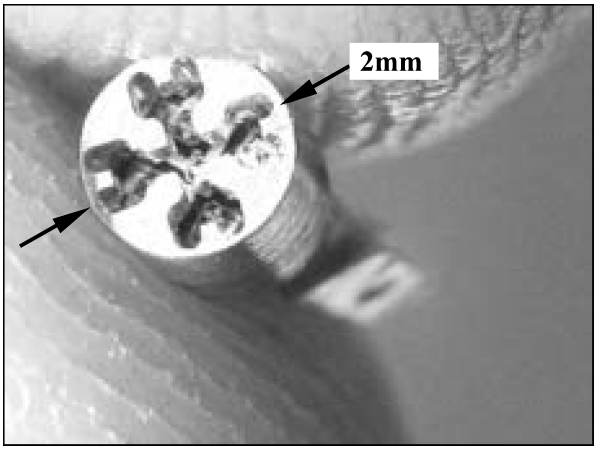

b)

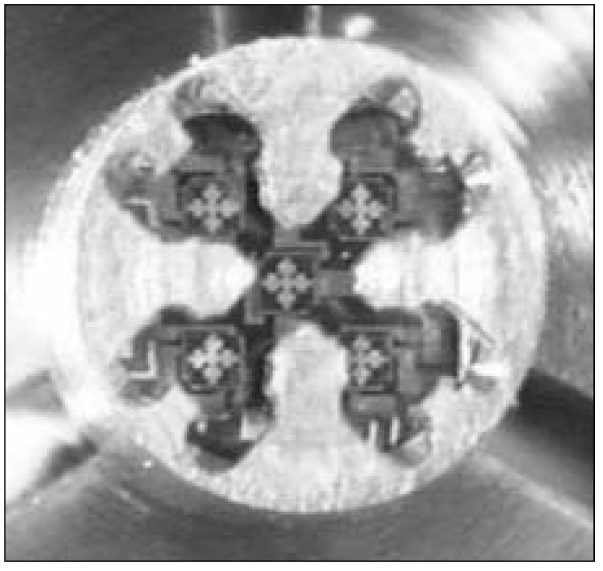

c)

Fig. 1 MEMS probe: a) schematic of the structure of a MEMS-based five-hole probe and b) and c) fabricated probe with its tip removed so that the internal details and MEMS sensors are revealed.

seven-hole probes with a tip diameter on the order of 1 mm, which in turn yields excellent spatial resolution. Figure 1 shows a schematic of the structure of a MEMS-based five-hole probe and pictures of the fabricated probe with its tip removed so that the internal details and MEMS sensors are revealed.[19]

Siddon[20] and Fuchs[21] undertook the challenging task of measuring the static pressure in an unsteady jet. Siddon[20] used a special probe that simultaneously determined the velocity magnitude and static pressure. He concluded that if the length scale of the unsteadiness is significantly larger than the probe size, the instantaneous, unsteady static pressures are negligibly different from the quasi-steady pressures. The unsteady stagnation pressures do not behave in the same manner. Based on potential flow theory, the pressure distribution over a sphere in an accelerated flowfield depends on both the instantaneous velocity and the rate of change of velocity.[22] The magnitude of the unsteady effect is proportional to the radius of the sphere and the flow acceleration and is inversely proportional to the square of the instantaneous velocity magnitude. Therefore, probes in flowfields with high-frequency fluctuations must be properly calibrated and the unsteady effects accounted for.

Kovasznay et al.[23] presented a theoretical and experimental investigation of the pressure distribution around a sphere in unsteady flowfields. They determined the velocity potential as the sum of three contributions: the potential caused by the steady flow over the sphere, the potential caused by the superimposed velocity disturbance, and the potential for the compensating flow, which was introduced to satisfy the boundary conditions. Based on this method, Matsunaga et al.[8] developed a theoretical procedure for calibrating a five-hole probe in unsteady conditions. The theoretical part of their algorithm, which consisted of the calculation of the perturbation potential around a perfect hemispherical tip, was not properly corrected to account for fabrication idiosyncrasies and imperfections of the specific probe. Senoo et al.[5] employed a three-hole cobra probe to measure two-dimensional instantaneous flow quantities at the exit of a pump impeller. Recognizing the difficulty of calibrating the probe in unsteady flow, they utilized the steady-state calibration of the probe to reduce the unsteady flow data. For their application, arguments were presented as to why this approach did not compromise the measurement accuracy, although no quantitatively unequivocal proof was presented.

In Gossweiler et al.,[24,25] Kupferschmied and Gossweiler,[26] and Kupferschmied et al.,[27] a four-hole, fast-response probe was designed for use in turbomachinery-related flows. The probe tip did not have any of the conventional geometries (conical or hemispherical) but was rather formed into a wedge, with a tip size of 2.5 mm and frequency response of 45 kHz. The unsteady aerodynamic effects on the probe calibration were not taken into account, and all data reductions were performed via the steady-steady probe calibration. The same group[28–30] tested several fast-response probe tip geometries in order to assess the measurement error when the quasi-steady probe calibration is used in accelerated flowfields. Several error sources were identified, the most important of which were inertial or apparent mass effects (potential flow effects), dynamic boundary-layer effects, dynamic-stall effects, and vortex-shedding effects. For a flow oscillation frequency of 5.9 kHz, depending on probe geometry and size (two probe tip sizes were tested, 4 and 8 mm), errors as high as 100% were identified. The highest errors were observed for wedge-type probe tip geometries, whereas circular probe tip geometries were found to reduce these errors dramatically (one order of magnitude). Another important result in Humm et al.[30] was the fact that for spherical tip geometries, the main two sources of errors were inertial (potential flow) effects and spatial velocity gradient effects. Viscosity and circulation-related errors were much smaller. From the preceding it is obvious that port pressures are subject to large unsteady aerodynamic effects. This means that if the probe is used in an unsteady flowfield and the steady probe calibration is used to estimate the instantaneous velocity vector from the instantaneously measured port pressures, significant errors can be made.

The unsteady inertial effects on a probe described in this work are estimated using potential flow theory. Furthermore, it will be shown here that the flow angle can be predicted with a high degree of accuracy using a set of nondimensional pressure coefficients that, in effect, cancel the inertial contributions in the measured port pressures. Using these coefficients, the flow angle can be accurately predicted without any direct quantification or correction of the inertial effects. Determination of the velocity magnitude, however, requires the quantification of the inertial contribution for at least one port (e.g., the center port). A procedure that utilizes steady and unsteady calibration coefficients and a numerical routine to

determine the velocity magnitude was derived. In this work, the algorithms are theoretically validated, using a theoretical probe with its operation based on potential flow theory. In subsequent parts of this effort,[31,32] water-tunnel and airjet facilities were developed that generate controlled, repeatable flow unsteadiness, and fast-response pressure probes were tested to experimentally verify the unsteady probe calibration algorithms developed herein.

Basic Theoretical Model

Consider a sphere in steady translation through an inviscid fluid at rest. The drag on this sphere is zero because of the equal and opposite pressure forces on the windward and the leeward sides of the sphere (d'Alembert's paradox). If the same sphere is in accelerated translation through the inviscid fluid, the pressure forces on the windward and leeward side no longer balance, and this results in a net force acting in the direction opposite to the acceleration. A multihole probe in an unsteady flowfield will also be subjected to these acceleration effects. This results in port pressures that are not only dependent on the dynamic pressure of the fluid and the tip geometry, but also on an additional term that is proportional to the flow acceleration. The following sections describe a method to quantify and correct these inertial effects such that a multihole probe can be successfully used in unsteady flowfields to predict the instantaneous velocity vector.

In steady, incompressible, irrotational flows, the relationship between pressure and velocity is governed by the steady Bernoulli equation:

$$p_t = p_s + \tfrac{1}{2}\rho U^2 = \text{const} \tag{1}$$

If one considers a sphere in accelerated translation through an infinite fluid at rest with a body-fixed reference frame (Fig. 2), the Bernoulli equation can be written as[22]

$$p(\boldsymbol{r}, t) = p_s - \rho\left[\frac{\partial \Phi}{\partial t} - \boldsymbol{U(t)} \cdot \nabla\Phi + \frac{1}{2}(\nabla\Phi)^2\right] \tag{2}$$

Equation (2) describes the pressure in the fluid in terms of the position vector $\boldsymbol{r}$ and time t. For a sphere, the flowfield is axisymmetric, and the position vector can be described in a spherical coordinate system in terms of r and θ (Fig. 2). The perturbation potential Φ is a scalar, the gradient of which yields the flow perturbation velocity. The velocity $\boldsymbol{U(t)}$ of the spherical surface, in spherical coordinates, is given as

$$\boldsymbol{U(t)} = U(t)\cos(\theta)\hat{r} - U(t)\sin(\theta)\hat{\theta} \tag{3}$$

For a sphere, the perturbation potential can be found by setting up the appropriate boundary conditions (no penetration) and solving the continuity equation using the method of separation of variables[22]:

$$\Phi(\theta, t) = -\tfrac{1}{2}U(t)(R^3/r^2)\cos(\theta) \tag{4}$$

where the radius of the sphere is given by R and $U(t)$ is the time-dependent velocity of the sphere. The pressure distribution on the sphere surface as a function of the sphere velocity and the angle θ is determined from Eq. (2). Calculating each of the terms in the unsteady Bernoulli equation and substituting back into Eq. (2) yields the following expression for the pressure distribution on the sphere surface:

$$p(\theta, U, t) = p_s + \frac{1}{2}\rho U(t)^2\left[\frac{9}{4}\cos^2(\theta) - \frac{5}{4}\right] + \frac{1}{2}\rho R\frac{\mathrm{d}U(t)}{\mathrm{d}t}\cos(\theta) \tag{5}$$

which can be written as

$$Cp(\theta, U, t) \equiv \frac{p(\theta, U, t) - p_s}{\frac{1}{2}\rho U(t)^2}$$

$$= \left[\frac{9}{4}\cos^2(\theta) - \frac{5}{4}\right] + \frac{R}{U(t)^2}\frac{\mathrm{d}U(t)}{\mathrm{d}t}\cos(\theta) \tag{6a}$$

This pressure coefficient is based on instantaneous velocities that can be described in terms of a steady and an unsteady component:

$$Cp(\theta, U, t) \equiv Cp_{\text{STEADY}} + Cp_{\text{UNSTEADY}} \tag{6b}$$

where

$$Cp_{\text{STEADY}} = \left[\frac{9}{4}\cos^2(\theta) - \frac{5}{4}\right] \tag{7a}$$

$$Cp_{\text{UNSTEADY}} = \frac{R}{U(t)^2}\frac{\mathrm{d}U(t)}{\mathrm{d}t}\cos(\theta) = K(t)\cos(\theta) \tag{7b}$$

This is the pressure distribution on the surface of the sphere, moving at velocity $U(t)$, in a fluid at rest. The same pressure distribution would also be seen if the sphere is stationary and the flowfield is moving with velocity $U(t)$. For steady flows, the inertial term described by Eq. (7b) vanishes, and the pressure distribution on the sphere surface is given by Eq. (7a). However, for accelerated flows the inertial term will be nonzero, and in the case of a multihole probe corrections must be made to accurately resolve the flow angle and velocity magnitude from the measured port pressures. On the windward side of a sphere, the viscous effects are small, and the pressure distribution is similar to the inviscid prediction. The general form of Eq. (6b) is assumed to describe the pressure distribution on the windward side of shapes that are consistent with spherical bodies, such as hemispheres or approximate hemispheres found on probe tips.

Two angle systems typically used for multihole probes are the cone-roll (θ, ϕ) angle system for the derivation of the inertial effects from potential flow and the pitch-yaw (α, β) angle system to describe the flow angle for a multihole probe. Figure 3 illustrates the

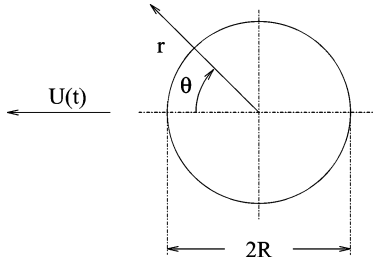

Fig. 2 Sphere accelerating in a fluid at rest.

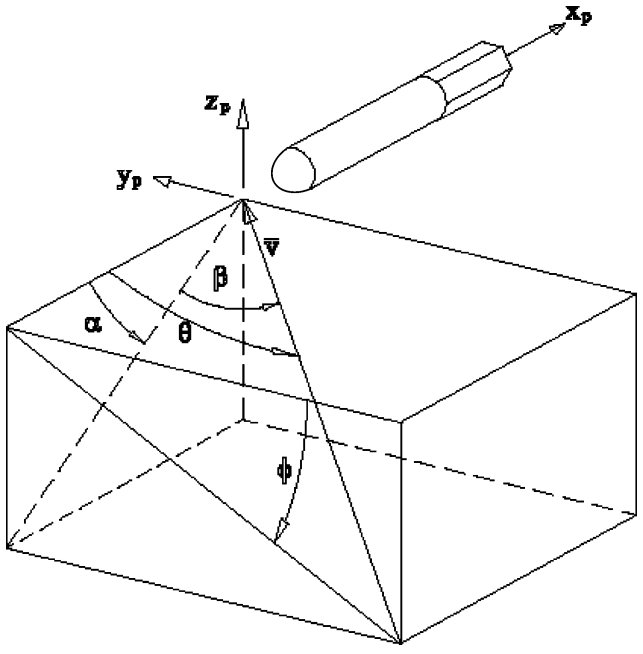

Fig. 3 Schematic representation of probe tip, velocity vector, and angle system definitions.

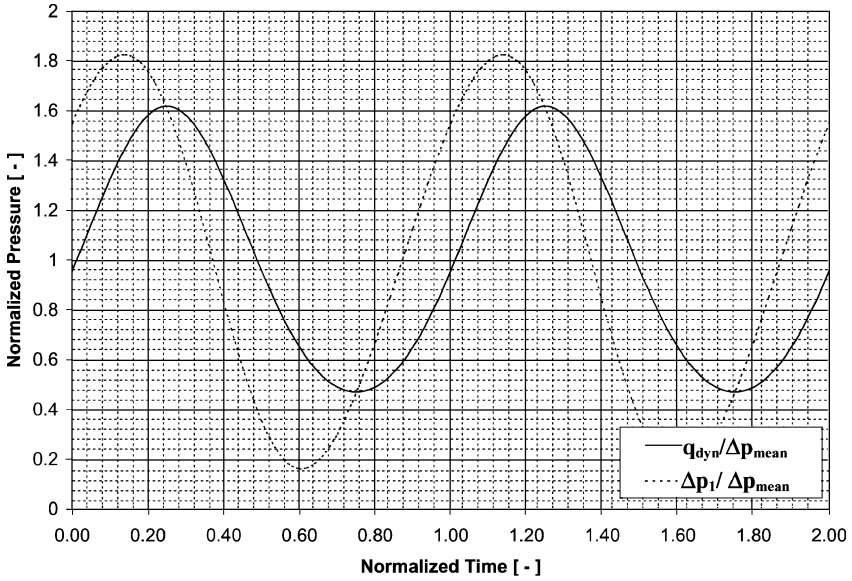

Fig. 4 Pressure at the forward stagnation point (with respect to static pressure) vs the true dynamic pressure of the fluid in the absence of the probe.

definitions of the two angle systems. The systems are completely interchangeable, and the conversion between the systems is given by geometry alone. For example, the conversion from the cone-roll angle system to the pitch-yaw angle system is given by

$$\alpha = \tan^{-1}(\tan\theta \sin\phi), \qquad \beta = \sin^{-1}(\sin\theta \cos\phi) \tag{8}$$

For the sphere, the inertial contribution has now been identified, and the pressure anywhere on its surface can be calculated for a steady or accelerated flowfield. The magnitude of the inertial contribution to the pressure on the sphere surface depends on the flow velocity, acceleration, and sphere diameter. To demonstrate the effects of the inertial term, consider the case of a 2-mm sphere (typical probe tip diameter) in a sinusoidally oscillating airstream with a mean velocity of 60 m/s, 30% amplitude, and frequency 20 kHz. Although the value used here for the oscillation amplitude (30%) is large and rather unrealistic, this number has been chosen in order to accentuate and clearly demonstrate the difference between the true and the measured dynamic pressure. The true instantaneous dynamic pressure of the flow (in the absence of the sphere) is given directly by

$$q_{\text{dyn}} = \tfrac{1}{2}\rho U(t)^2 \tag{9a}$$

The pressure that would exist at the forward stagnation point on the sphere surface (indicated as Δp_1 in Fig. 4) is given by Eq. (5) (for $\theta = 0$):

$$\Delta p_1(\theta, U, t) = p_1(\theta, U, t) - p_s = \frac{1}{2}\rho U(t)^2 + \frac{1}{2}\rho R\frac{\mathrm{d}U(t)}{\mathrm{d}t} \tag{9b}$$

Plotting these two pressures (nondimensionalized with the mean value of Δp_1) vs time reveals that the pressure on the sphere is larger in amplitude and leads the flow dynamic pressure in phase (Fig. 4). It is also seen that the pressure on the sphere crosses the true dynamic pressure at the peaks and the valleys, where the flow acceleration is zero.

Comparison of the Theoretical Model and a Real Probe

A multihole probe can be theoretically modeled as a sphere with ports at known angular locations. If this modeled probe is placed in a flowfield with given flow angle, velocity, and acceleration, the corresponding port pressures can be found from Eqs. (6a) and (6b) by properly accounting for the angular offset in the port locations. To justify this approach, it is shown in this section that such a modeled probe has a steady flow pressure distribution very similar to a hemispherical tipped five-hole probe in the low flow angle range.

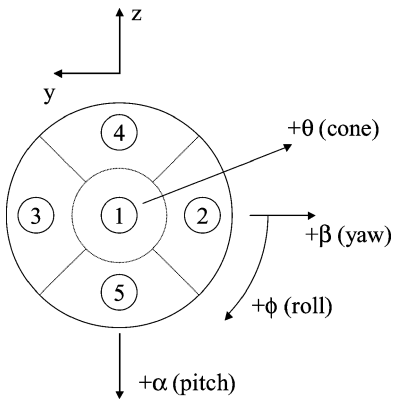

Fig. 5 Port numbering and definition of angle system for five-hole probe.

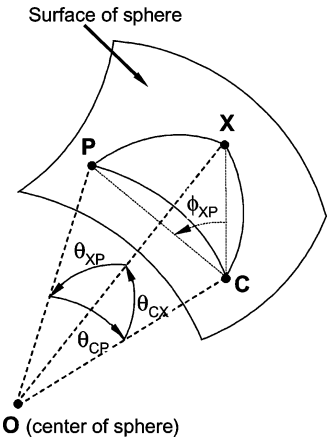

Fig. 6 Schematic to aid in the determination of the port pressures from the incidence angle.

A five-hole probe typically has a central pressure port and four peripheral pressure ports. Here, we consider a five-hole probe with the port numbering shown in Fig. 5. The theoretical/modeled probe has a center port and four peripheral ports located at a fixed cone angle (33 deg) and roll angles of 0, 90, 180, and 270 deg (Fig. 5). Equations (6a) and (6b) can be modified such that each of the pressure ports has an associated expression that relates the flow velocity and angularity with the measured port pressure. In the previous analysis, relating to Fig. 2, the stagnation point was known and fixed;

therefore, only one variable, angle θ, was enough to describe the pressure anywhere on the sphere surface. Now, however, as the flow angle with respect to the probe axis changes, the stagnation point changes location as well. Thus, in order to describe the relative position of the stagnation point with respect to a pressure port two variables, the pitch and yaw angles, α and β, are necessary. Also note that the pitch and yaw angles, α and β, are global with respect to the probe axis and not local, with respect to the individual ports:

$$Cp(\alpha, \beta, U, t)_i \equiv \frac{p_i(\alpha, \beta, U, t) - p_s}{\frac{1}{2}\rho U(t)^2} = Cp_{\text{STEADY}_i} + Cp_{\text{UNSTEADY}_i} \tag{10}$$

where i indicates the ith port of the multihole probe. In Fig. 6, the pressure port i is denoted with P, the forward center port with C, and the flow stagnation point with X. O denotes the center of the sphere, and all lengths OC, OP, and OX are equal to the radius of the sphere R. From geometry, the angle θ_{XP} is given by

$$\theta_{\text{XP}} = 2\sin^{-1}\left\{\left[\sin(\theta_{\text{CP}}/2)^2 + \sin(\theta_{\text{CX}}/2)^2 - 2\sin(\theta_{\text{CP}}/2)\sin(\theta_{\text{CX}}/2)\cos(\phi_{\text{XP}})\right]^{-\frac{1}{2}}\right\} \tag{11}$$

where θ_{CP} and θ_{CX} are the cone-angle positions of the pressure port P and stagnation point X, respectively, with respect to the central pressure port C. ϕ_{XP} is the roll-angle difference between the port location P and the stagnation point X.

The steady port pressures for the modeled probe were then compared with the calibration of a 3.2-mm-diam, hemispherical-tip five-hole probe with port numbering identical to that of Fig. 5 and pressure port diameter of 0.3 mm. The probe has an approximate hemispherical shape, and each pressure port is not infinitesimally small but spans a relatively significant surface area (port diameter is about 1/11th of the probe diameter). The peripheral pressure ports have their centers at approximately $\theta = 33$ deg. This probe was calibrated in a wind tunnel at 30 m/s using a cone-roll probe positioning system. The theoretical model was used to calculate the five port pressures for the same angle combinations as in the actual calibration file. In Figs. 7–9, the calculated and experimental center port (port 1), port 2, and port 3 pressures are compared. Bearing in mind that the probe is actually a hemisphere-cylinder and not a sphere, that the actual probe tip is not a perfect hemisphere (because of manufacturing imperfections, especially at these small tip sizes), and that the ports have a finite size and their cone location is not precisely 33 deg, the agreement is quite good, especially for cone angles below 40 deg. The significant differences above 40 deg are because

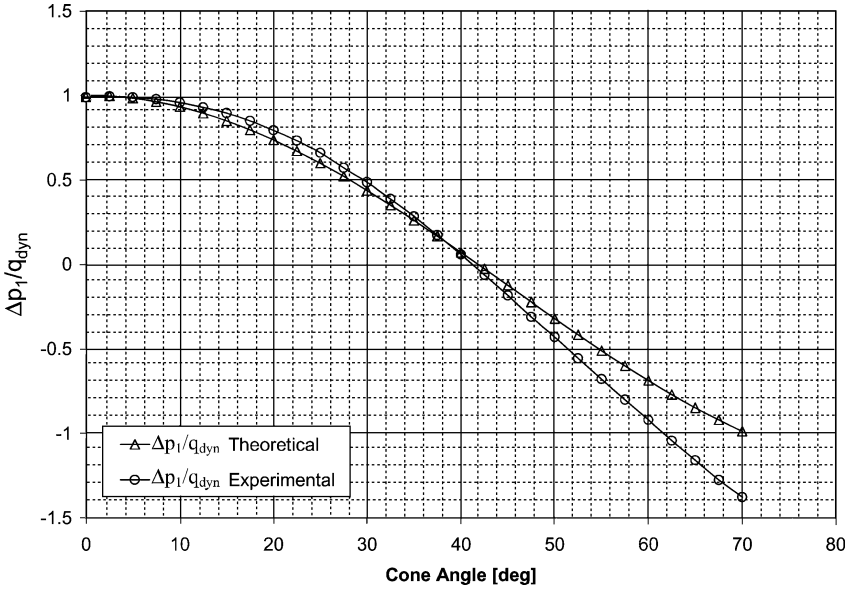

Fig. 7 Theoretical and experimental center port (port 1) pressures for roll angle of 0 deg.

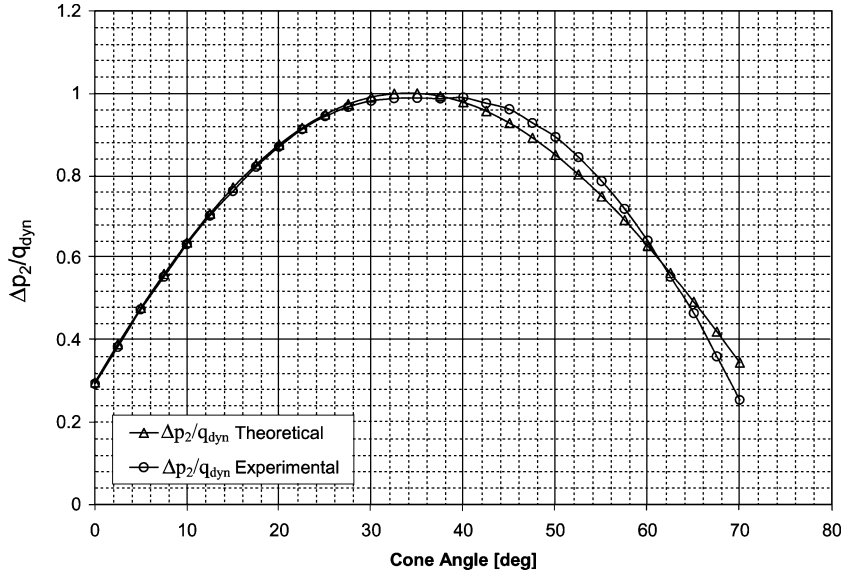

Fig. 8 Theoretical and experimental port 2 pressures for roll angle of 0 deg.

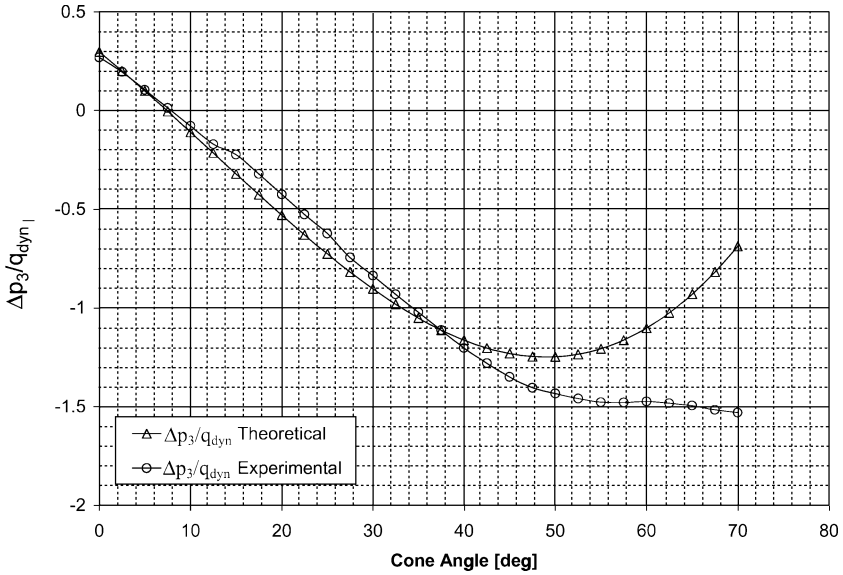

Fig. 9 Theoretical and experimental port 3 pressures for roll angle of 0 deg.

for these angles some of the ports in the actual probe experience laminar flow separation (the Reynolds number based on the probe diameter is around 6.4×10^3), whereas the theoretical predictions (potential flow) do not account for that.

Parameters for Time-Dependent Flowfields

Some assumptions must be made at this point. There can be no spatial velocity gradients of the oncoming flow over distances equal to the probe diameter, which leads to the restriction that the wavelength of the unsteadiness in the oncoming flow must be significantly larger than the size of the probe[23]:

$$R \ll \lambda \tag{12}$$

where λ is the wavelength of the disturbance. Furthermore, it shall be assumed that the flow oscillations are purely axial (i.e., there are no angular oscillations in the flowfield). The reason for that is the fact that angular oscillations do not contribute to inertial effects. In an aerodynamic design study of probe geometries, Humm et al.[30] found that for cylinders there are negligible circulation-induced effects from angular oscillations, and it is reasonable to believe that these results are also valid for a sphere or a hemisphere. Therefore, the probe should be able to resolve flows in which angular oscillations are present, assuming again that this results in no significant velocity gradients of the oncoming flow over the probe diameter. To characterize unsteady flows, a nondimensional frequency ω^* has traditionally been used:

$$\omega^* = 2R\omega/\bar{U} \tag{13}$$

However, for general, nonperiodic flows, an instantaneous nondimensional acceleration K is better suited to nondimensionalize Eq. (6):

$$K(t) = \frac{R}{U(t)^2}\frac{\mathrm{d}U(t)}{\mathrm{d}t} \tag{14}$$

With this, and in order to express Cp as a function of $K(t)$, we rewrite Eq. (6a) as follows:

$$Cp[\alpha, \beta, K(t)] = Cp_S(\alpha, \beta) + K(t)Cp_U(\alpha, \beta) \tag{15a}$$

where

$$Cp_{\text{STEADY}} = Cp_S, \qquad Cp_{\text{UNSTEADY}} = K(t)Cp_U \tag{15b}$$

and for the theoretical sphere and analysis of Fig. 2,

$$Cp_S = \left[\tfrac{9}{4}\cos^2(\theta) - \tfrac{5}{4}\right], \qquad Cp_U = \cos(\theta) \tag{15c}$$

The nondimensional acceleration K describes the magnitude of the unsteady or inertial effects on the probe. This nondimensional acceleration for a periodic flow will also be periodic; hence, it is not a constant like the nondimensional frequency ω^*. If all flows were sinusoidal, it would be easy to define K in such a way that it would be a constant for a specific flow (not a function of time) and would also have a clear analytical expression in terms of the frequency of oscillation, the amplitude of oscillation, and the probe radius {such a parameter could be, for example, the rms of the K defines in Eq. (14), that is, $K_{\text{RMS}} = \langle [R/U(t)^2][\mathrm{d}U(t)/\mathrm{d}t] \rangle$}. However, for a generic unsteady flow (nonsinusoidal, or not even periodic), although the quantity $K_{\text{RMS}} = \langle [R/U(t)^2][\mathrm{d}U(t)/\mathrm{d}t] \rangle$ can still be defined, it cannot be analytically expressed in terms of the flow unsteadiness parameters. Another definition, which is also more conservative than the definition of K_{RMS} could be

$$K_{\text{MAX}} = \text{MAX}\left[\frac{R}{U(t)^2}\frac{\mathrm{d}U(t)}{\mathrm{d}t}\right]$$

From the expressions in Eqs. (14) and (15), it can be seen that the error $Cp[\alpha, \beta, K(t)] - Cp_S(\alpha, \beta)$, made by ignoring the inertial term, is linearly proportional to K or, equivalently, linearly proportional to the probe size and the acceleration and inversely proportional to the square of the velocity. To demonstrate the point, consider the probe of our last example (tip diameter of 2 mm) placed in an oscillating airstream at zero incidence angle. The flow velocity is taken to be sinusoidal with a frequency of 2 kHz, a mean of 20 m/s, and 10% amplitude. The value of the nondimensional acceleration coefficient is identical to the error in magnitude if the inertial effects are ignored. For our example, the calculated maximum K value is 0.063, meaning that for the 2-mm probe in the described flowfield a maximum measurement error in the predicted dynamic pressure of 6.3% is expected if the inertial effects are not accounted for. If the frequency is increased to 20 kHz, the maximum error in the predicted dynamic pressure will increase to 63%.

Calculation of the Flow Angles

For measurements in steady flows, steady probe calibration is first performed to determine the relationship between the port pressures and the flow incidence angle. The port pressures are used to form two nondimensional pressure coefficients, B_α and B_β, that describe this relationship. Based on the port numbering in Fig. 5, the definitions of B_α and B_β are given in terms of the port pressures p_i as

$$B_\alpha = \frac{p_5 - p_4}{p_1 - \frac{1}{4}(p_2 + p_3 + p_4 + p_5)} \tag{16}$$

$$B_\beta = \frac{p_2 - p_3}{p_1 - \frac{1}{4}(p_2 + p_3 + p_4 + p_5)} \tag{17}$$

The probe is first calibrated in a steady flowfield where it is pitched and yawed through a range of angles to simulate all possible flow inclinations. For each angle the port pressures are recorded, and the coefficients are calculated. Polynomial surface fits that express the flow angles α or β as functions of the pressure coefficients B_α and B_β are created. For steady data reduction in an unknown flowfield, the pressure coefficients B_α and B_β are calculated from the measured port pressures. The pitch and yaw angles of the flow are then given directly by their respective polynomial expressions. This procedure is well established for steady probe calibration and data reduction,[1–4] but in an unsteady flowfield the individual pressures that compose these coefficients also contain inertial effects [Eq. (5)].

Similarly, an additional set of independent pressure coefficients can be defined for high-angle flows; however, the present discussion will be limited to low-angle flows (i.e., where the central pressure port has the highest pressure). Using the expressions in Eqs. (16) and (17) and dividing throughout with the dynamic pressure $(1/2\rho U^2)$, the coefficients B_α and B_β can be expressed in terms of pressure coefficients similar to those in Eq. (15a).

B_α and B_β, in terms of the steady and unsteady pressure coefficients, are given as

$$B_\alpha[\alpha, \beta, K(t)] = \frac{Cp_{S_5}(\alpha,\beta) - Cp_{S_4}(\alpha,\beta) + K(t)\left[Cp_{U_5}(\alpha,\beta) - Cp_{U_4}(\alpha,\beta)\right]}{Cp_{S_1}(\alpha,\beta) - \frac{1}{4}\sum_{i=2}^{5} Cp_{S_i}(\alpha,\beta) + K(t)\left[Cp_{U_1}(\alpha,\beta) - \frac{1}{4}\sum_{i=2}^{5} Cp_{U_i}(\alpha,\beta)\right]} \tag{18}$$

$$B_\beta[\alpha, \beta, K(t)] = \frac{Cp_{S_2}(\alpha,\beta) - Cp_{S_3}(\alpha,\beta) + K(t)\left[Cp_{U_2}(\alpha,\beta) - Cp_{U_3}(\alpha,\beta)\right]}{Cp_{S_1}(\alpha,\beta) - \frac{1}{4}\sum_{i=2}^{5} Cp_{S_i}(\alpha,\beta) + K(t)\left[Cp_{U_1}(\alpha,\beta) - \frac{1}{4}\sum_{i=2}^{5} Cp_{U_i}(\alpha,\beta)\right]} \tag{19}$$

In Eqs. (18) and (19), the nondimensional acceleration K appears in both the numerator and denominator. The theoretical sphere-based probe is used to calculate these expressions for B_α and B_β as functions of the nondimensional acceleration K. For a K value of zero, the expressions reduce to the steady definitions. The behavior of B_β, for example, is shown in Fig. 10, and is quite remarkable. The B_β coefficient (the same holds for coefficient B_α as well) shows very little dependence on the inertial effects for yaw angles between -30 and 30 deg, even for large values of K. As mentioned earlier, the low-angle definition of B_β is never used for angles larger than about 25 deg. Figure 11 shows the difference between the steady and unsteady B_β coefficients as a percentage of the range of B_β, for yaw angles between -20 and 20 deg for K values from 0 to ± 0.5. Figure 12 shows the error in B_α and B_β (percentage of the full range) if the inertial effects are ignored, for a range of pitch and yaw angles from -20 to $+20$ deg and a constant K value of 1.0. Even for this extreme value of K, there is little impact of the inertial effects on the measured coefficient values.

As seen in Figs. 11 and 12, the inertial effects barely affect the value of the B_β coefficient. This further enables the use of the steady calibration polynomial surface fits to be used in the prediction of the flow angles of an unknown, unsteady flowfield. The port pressures, which can contain significant inertial effects individually, are used to calculate the independent pressure coefficients from Eqs. (16) and (17). Because, as shown, these coefficients are insignificantly influenced by inertial effects, they can be used to determine the flow angles directly from the steady polynomial expressions. Therefore, no inertial correction is necessary to determine the flow angles using this procedure:

$$\alpha(B_\alpha, B_\beta)|_{\text{unsteady}} \approx \alpha(B_\alpha, B_\beta)|_{\text{steady}} \tag{20}$$

$$\beta(B_\alpha, B_\beta)|_{\text{unsteady}} \approx \beta(B_\alpha, B_\beta)|_{\text{steady}} \tag{21}$$

This simplifies the task of resolving the flowfield. It must be reiterated that a K value of 0.5 (Fig. 11) is very large (for moderate flow velocities), and the errors observed in Fig. 11 for $K = 0.5$ represent a rather extreme case. The error in degrees that results from the error in the independent pressure coefficients is dependent on the actual flow angle, but is within the well-established prediction capabilities of a steady probe, even for very large unsteady effects (large K values).

Consider the theoretical model for a spherical five-hole probe with a tip diameter of 2 mm, placed in a flow with a mean velocity of 30 m/s with a sinusoidal oscillation of $\pm 20\%$ and frequency of 11 kHz. Although these parameters do not necessarily correspond to a realistic flow, they were deliberately exaggerated to illustrate the point that even in cases with significant inertial effects the prediction

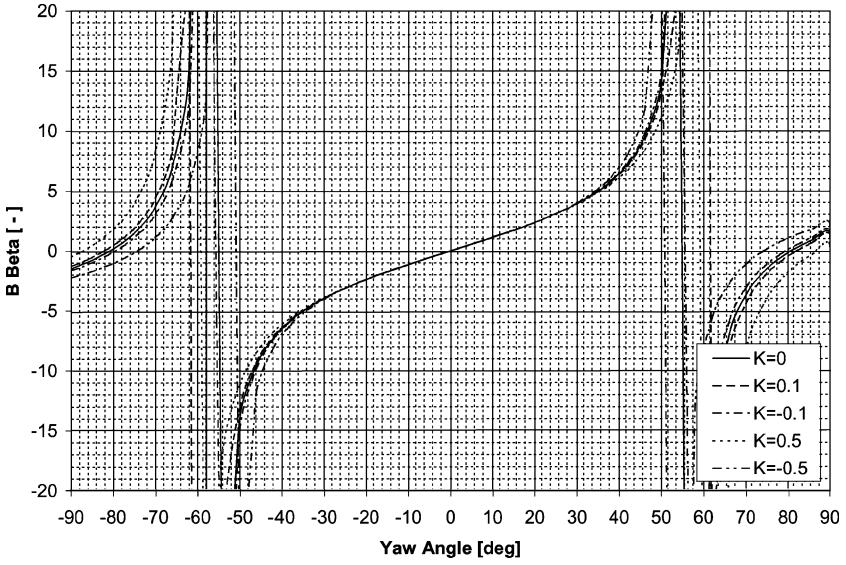

Fig. 10 Nondimensional coefficient B_β vs yaw angle and its dependence on the unsteadiness parameter K.

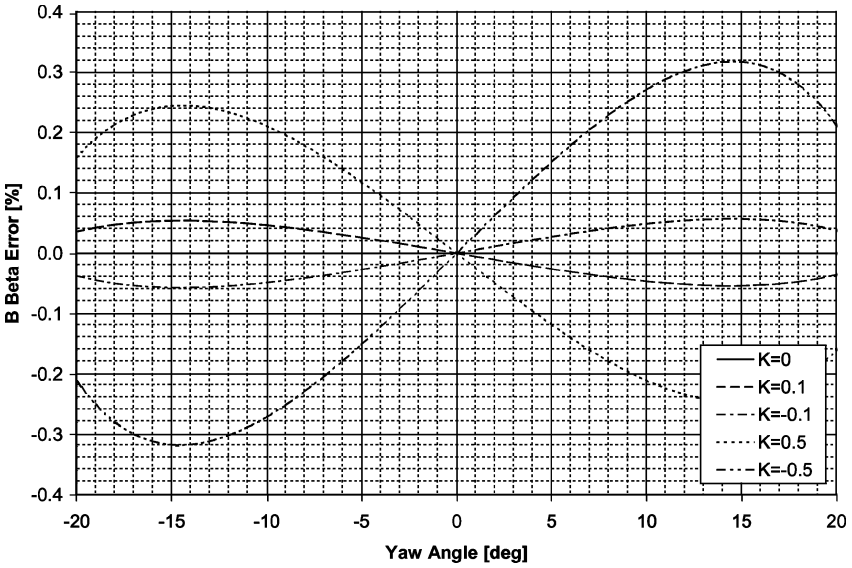

Fig. 11 Difference between the steady and unsteady definitions of B_β vs yaw angle. The difference is given as a percentage of the range of B_β.

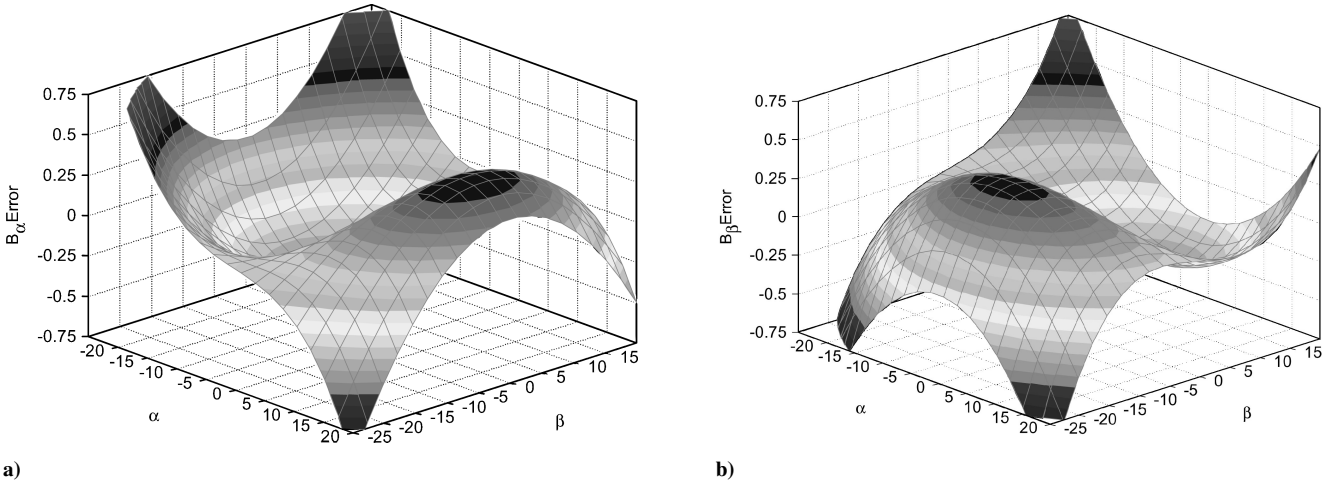

a) b)

Fig. 12 Difference between steady and unsteady definitions of a) B_α and b) B_β over a range of pitch and yaw angles from −20 to 20 deg and constant $K = 1.0$. The difference is given as a percentage of the range of B_α and B_β.

of the flow angles can be very accurate. Let us assume the flow angles are 0 deg pitch (α) and 15 deg yaw (β). The steady independent pressure coefficients were first calculated (from the theoretical pressure coefficient for a sphere) for this probe. Subsequently, time series of the five unsteady pressures were calculated for the particular flowfield. The unsteady independent pressure coefficients B_α and B_β were then calculated from Eqs. (18) and (19). The time series for the instantaneous flow angles were calculated from Eqs. (20) and (21). The error between the instantaneous predicted and exact flow angles is shown in Fig. 13. To understand why the error in the pitch-angle prediction is exactly zero, we should look at Eq. (18). For zero pitch flow angle, the pressure coefficients for ports 4 and 5 (both steady and unsteady coefficients) are equal (because of symmetry). Therefore, the numerator in Eq. (18) is zero regardless of the magnitude of K, that is, regardless of the magnitude of the unsteady effects. For all other values of pitch flow angle, the influence of the unsteady term depends on both the angle and K. This is the case here for the yaw angle, which therefore does not have an identically zero error. As seen here, even for high K values (± 0.5 in this example) the mean error is very small.

The calculations in the preceding example were purely theoretical and were based on a perfect spherical probe, not an imperfect hemisphere on a real probe. However, given the agreement between theoretical and experimental values for steady data (Figs. 7 to 9), the procedure should also be valid for a real probe granted accurate steady calibration data are available. (This statement will be validated in Refs. 31 and 32.) However, it is reasonable to believe that the excellent results are as a result of the perfect symmetry of the probe. Therefore, an analysis was performed where each of the pressure port locations were perturbed, even beyond the ranges that would be seen for a real five-hole probe. The surface remains a perfect hemisphere, but the symmetry and the possible "canceling effect" from diametrically opposing pressure ports are no longer present. The perturbed pressure port locations are given in Table 1. The theoretical steady calibration of the probe reflects the effects of the introduced port asymmetry. A time series of data with the same parameters as in the preceding example was created for the perturbed

Table 1 Original and perturbed port locations

	Original		Perturbed	
Port no.	Cone, deg	Roll, deg	Cone, deg	Roll, deg
1	0	0	1	0
2	33	0	37	4
3	33	180	28	170
4	33	90	35	93
5	33	270	32	268

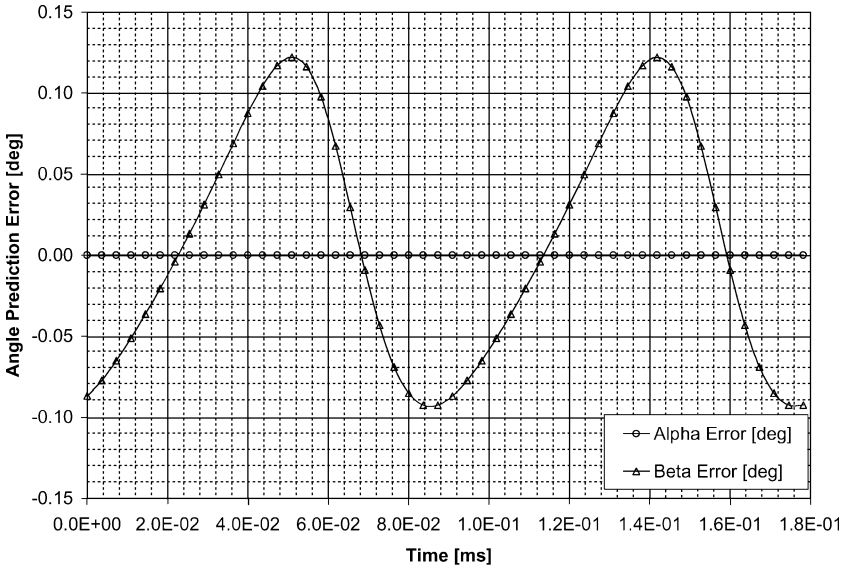

Fig. 13 Error in predicted pitch and yaw angles in degrees. The mean offset error depends on the flow incidence angle as well as the rate-of-change coefficient K.

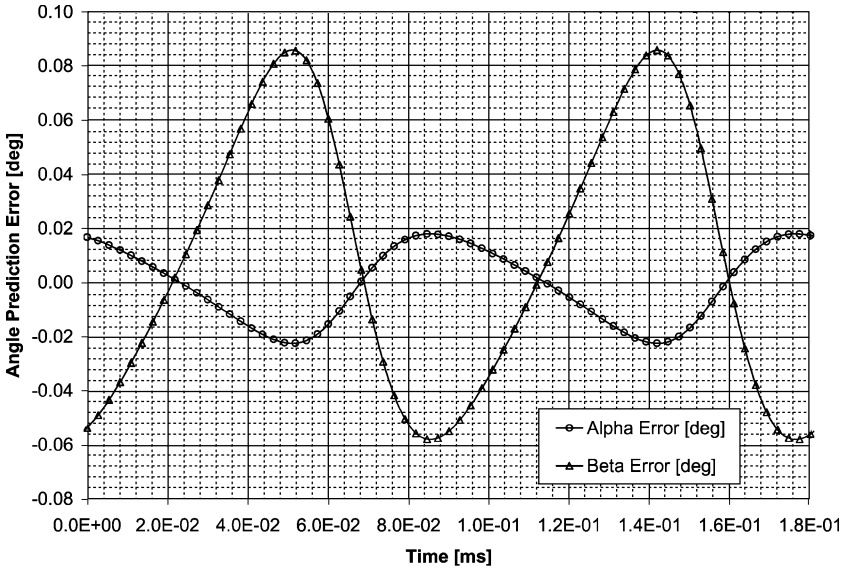

Fig. 14 Error in predicted pitch and yaw angles in degrees for a perturbed probe.

probe and the same procedures, as in the preceding example, were followed. The error between the instantaneous predicted and exact flow angles is shown in Fig. 14. For the unperturbed probe there was no error in the predicted pitch angle; however, for the perturbed probe a small periodic pitch error was observed. An important observation is that the range of the yaw error does not increase from the unperturbed to the perturbed case. (The range of yaw error has actually decreased slightly.) This shows that the prediction capabilities are not dependent upon port location symmetry (as long as accurate steady calibration is available).

However, as it will be seen next, this independence of the flow angles from inertial effects is not shared by the velocity magnitude. Correct measurement of the velocity magnitude requires exact quantification of the inertial effects.

Calculation of Velocity Magnitude

The velocity magnitude for a conventional (steady) multihole probe is generally calculated from the total and static pressures. These pressures are determined, via the probe's steady calibration, from the measured port pressures. For probe use in an unsteady flowfield, the introduced procedure for determining the instantaneous velocity magnitude is described next. For this work, and without loss of generality,[19] the static pressure will be assumed to be known, but not necessarily constant. From Eq. (15a), the center port pressure is given as

$$\frac{p_1(\alpha, \beta, U, t) - p_s}{\frac{1}{2}\rho U(t)^2} = Cp_{S_1}(\alpha, \beta) + K(t)Cp_{U_1}(\alpha, \beta) \qquad (22)$$

For a perfect sphere and potential flow, Cp_S and Cp_U are given by Eq. (15c) (for a theoretical sphere) in a cone-roll angle system and can be easily converted in a pitch-roll angle system. From the steady probe calibration, the true or experimental steady pressure coefficient Cp_S can be found vs the pitch and yaw angles by

$$Cp_{S_1}(\alpha, \beta) = \frac{p_1(\alpha, \beta) - p_s}{\frac{1}{2}\rho U(t)^2} \qquad (23)$$

The experimental determination of the unsteady pressure coefficient is challenging[19] and is addressed in Refs. 31 and 32. For now, it will be assumed that such an expression can be found and can be

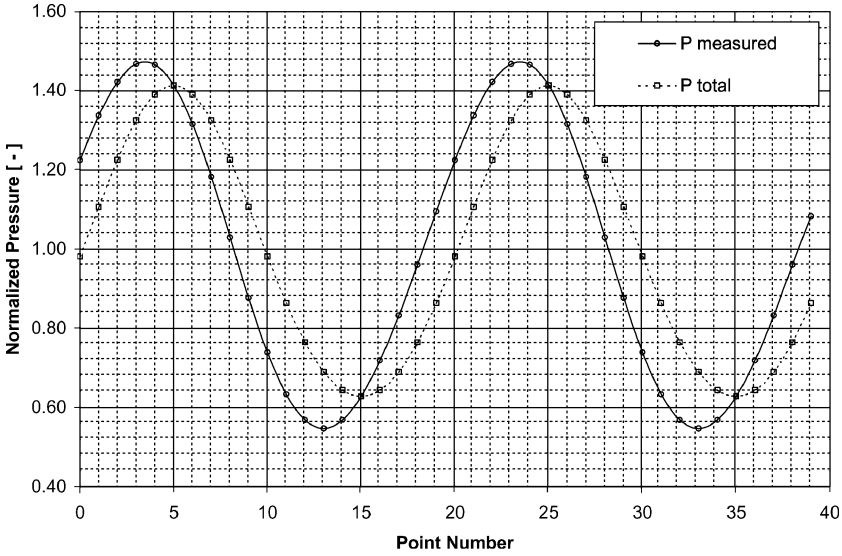

Fig. 15 Normalized sphere pressure and total pressure (both with respect to freestream static pressure) of the flow with 20 points per period.

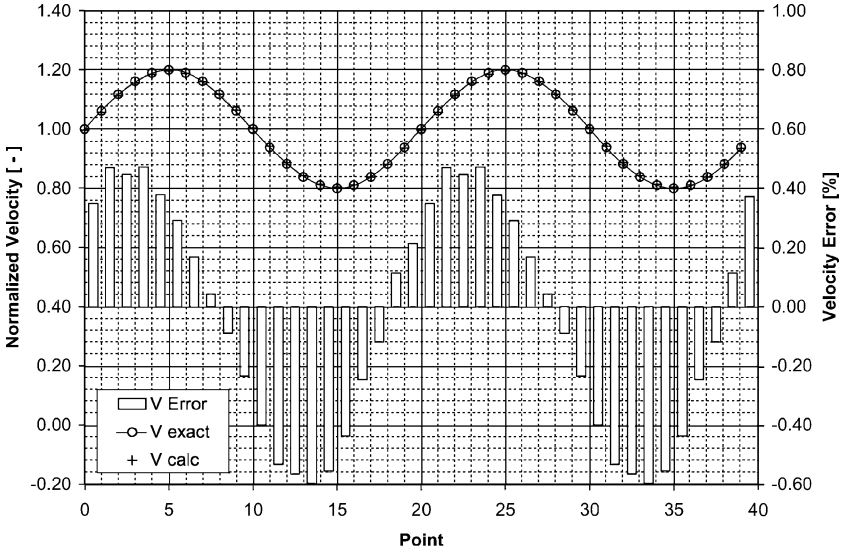

Fig. 16 Velocity prediction based on the numerical method with 20 points per period.

put in the form of a polynomial of the pitch and yaw angles. During data reduction, time series of the port pressures $p_i(t)$ are recorded, and the pitch and yaw angles are found for each time instant (from the preceding section on flow-angle determination). Based on these predicted angles, the steady and unsteady pressure coefficients are found from their respective polynomial expressions. The velocity is found by solving Eq. (6a), which is a nonlinear, first-order, ordinary differential equation. Such equations can easily be solved for a time series of data using a numerical method, such as the Runge–Kutta method. The first step in obtaining a solution for the velocity time series is to find the best possible prediction for the velocity at the start of the time series. However, with no a priori knowledge of the flowfield a good prediction of the starting velocity is nearly impossible. Fortunately, although reasonable starting guesses will help, they are not necessary in determining the velocity for a time series. The starting value can be set as (ignoring inertial effects)

$$U(t_0) = \sqrt{\frac{2p_1(t_0)}{\rho C p_S[\alpha(t_0), \beta(t_0)]}} \tag{24}$$

Generally, after evaluating the derivative from Eq. (6), a Taylor-series expansion could be used to determine the velocity at the second time instant t_1. However, because it is probable (at least for large K values) that a poor guess was made for the first time instant t_0 this extra complication is unwarranted, and the velocity at t_1 will also be set similar to Eq. (24).

Consider a probe in a sinusoidally varying flowfield with oscillation amplitude of 20% and maximum K value of 0.25. The normalized measured and total pressures are shown in Fig. 15, revealing significant inertial effects. The sampling rate is 20 points per period. As mentioned, the starting point of the time series is a problem area, and two periods were therefore discarded from the start of the time series. Figure 16 shows the predicted velocity magnitude and the error in the predicted velocity magnitude. As observed in the figure, the accuracy of the method is quite good. Increasing the sampling rate decreases the error of the numerical technique. A doubling of the sampling rate to 40 points per period results in maximum predicted velocity errors of 0.1%, a significant improvement from the 20 points-per-period results.

Conclusions

Multihole probes have traditionally been restricted to steady flowfields because of several unresolved issues in their response to unsteady flowfields, such as issues pertaining to unsteady aerodynamic effects on probe calibration. As a result of these effects, when

the probe is used in a dynamically changing flowfield the steady probe calibration can generally not be used directly to accurately reduce the instantaneous measured pressures to the instantaneous velocity vector. This work presents the theoretical background of a procedure to quantify and correct for the most important unsteady aerodynamic effect, namely, inertial effects. Based on potential flow, a theoretical probe was studied, and the unsteady effects were quantified in terms of a single nondimensional time-dependent coefficient K, which is a function of probe size, mean flow velocity, and flow acceleration. Subsequently, a set of flow angle pressure coefficients were introduced and were shown to be nearly independent of inertial effects such that the flow angles can be accurately predicted without any inertial corrections. Determination of the velocity magnitude, however, requires the determination of the magnitude of the inertial contribution from at least one port pressure. The governing equation, which is a first-order, nonlinear, ordinary differential equation was solved using a numerical procedure (Runge–Kutta). Both flow angle and velocity magnitude prediction procedures were demonstrated, for a theoretical five-hole probe, and exhibited very good prediction accuracy.

Acknowledgments

This work was sponsored by the Air Force Office of Scientific Research under Grant/Contract F49620-98-1-0162. The authors thank Thomas Beutner, the Technical Monitor of the project, as well as his predecessor, Mark Glauser. The work was also supported by Aeroprobe Corporation under Project 32500-7260M. The authors also thank Rick Allen for building the probes and support hardware as well as Lance Traub for his help with this work.

References

[1]Bryer, D. W., and Pankhurst, R. C., "Pressure-Probe Methods for Determining Wind Speed and Flow Direction," Her Majesty's Stationery Office/National Physics Lab., Campfield Press, St. Albans, England, U.K., 1971.

[2]Everett, K. N., Gerner, A. A., and Durston, D. A., "Seven-Hole Cone Probes for High Angle Flow Measurements: Theory and Calibration," *AIAA Journal*, Vol. 21, No. 7, 1983, pp. 992–998.

[3]Rediniotis, O. K., Hoang, N. T., and Telionis, D. P., "The Seven-Hole Probe: Its Calibration and Use," *Forum on Instructional Fluid Dynamics Experiments*, Vol. 152, 1993, pp. 21–26.

[4]Zilliac, G. G., "Calibration of Seven-Hole Probes for Use in Fluid Flows with Large Angularity," NASA TM 102200, Dec. 1989.

[5]Senoo, Y., Kita, Y., and Ookuma, K., "Measurement of Two-Dimensional Periodic Flow with a Cobra Probe," *Journal of Fluids Engineering*, June 1973, pp. 295–300.

[6]Castorph, D., and Raabe, J., "Measurement of Unsteady Pressure Unsteady Relative Velocity Field of a Kaplan Runner by Means of an Electronic Multi-Miniature Probe as a Basic Contribution to Research on Unsteady Runner Load," *Proceedings of the 7th IAHR Symposium*, edited by K. S. Tickle, C. Xu, I. C. Goulter, and S. Wasimi, A. A. Balkema, Leiden, The Netherlands, 1974.

[7]Kerrebrock, J. L., Thompkins, W. T., and Epstein, A. H., "A Miniature High Frequency Sphere Probe," *Proceedings of the Joint Fluids Engineering Gas Turbine Conference and Products Show*, American Society of Mechanical Engineers, New York, 1980, pp. 91–97.

[8]Matsunaga, S., Ishibashi, H., and Nishi, M., "Measurement of Instantaneous Pressure and Velocity in Nonsteady Three-Dimensional Water Flow by Means of a Combined Five-Hole Probe," *Journal of Fluids Engineering*, Vol. 102, June 1980, pp. 196–202.

[9]Ng, W. F., and Popernack, T. G., Jr., "Combination Probe for Hi-Frequency Unsteady Aerodynamic Measurements," *IEEE Transactions on Aerospace and Electronic Systems*, Vol. 24, No. 1, 1988, pp. 76–84.

[10]Naughton, J. W., Cattafesta, L. N., III, and Settles, G. S., "A Miniature, Fast-Response 5-Hole Probe for Supersonic Flowfield Measurements," AIAA-92-0266, Jan. 1992.

[11]Naughton, J. W., Cattafesta, L. N., III, and Settles, G. S., "Miniature Fast Response Five-Hole Conical Probe for Supersonic Flowfield Measurements," *AIAA Journal*, Vol. 31, No. 3, 1993, pp. 453–458.

[12]Roduner, C., Koppel, P., Kupferschmied, P., and Gyarmathy, G., "Comparison of Measurement Data at the Impeller Exit of a Centrifugal Compressor Measured with Both Pneumatic and Fast-Response Probes," American Society of Mechanical Engineers, Paper 98-GT-241, 1998.

[13]Roduner, C., Kupferschmied, P., Koppel, P., and Gyarmathy, G., "On the Development and Application of the Fast-Response Aerodynamic Probe System in Turbomachines—Part 2: Flow, Surge, and Stall in a Centrifugal Compressor," *Journal of Turbomachinery*, Vol. 122, July 2000, pp. 517–526.

[14]Koppel, P., Roduner, C., Kupferschmied, P., and Gyarmathy, G., "On the Development and Application of the Fast-Response Aerodynamic Probe System in Turbomachines—Part 3: Comparison of Averaging Methods Applied to Centrifugal Compressor Measurements," *Journal of Turbomachinery*, Vol. 122, July 2000, pp. 527–536.

[15]Kupferschmied, P., Koppel, P., Roduner, C., and Gyarmathy, G., "On the Development and Application of the Fast-Response Aerodynamic Probe System in Turbomachines—Part 1: The Measurement System," *Journal of Turbomachinery*, Vol. 122, July 2000, pp. 505–516.

[16]Kupferschmied, P., Koppel, P., Gizzi, W., Roduner, C., and Gyarmathy, G., "Time-Resolved Flow Measurements with Fast-Response Aerodynamic Probes in Turbomachines," *Measurement Science and Technology*, Vol. 11, 2000, pp. 1036–1054.

[17]Rediniotis, O. K., Johansen, E. S., Tsao, T., Seifert, A., and Pack, L. G., "MEMS-Based Probes for Velocity and Pressure Measurements in Unsteady and Turbulent Flowfields," AIAA Paper 99-0521, Jan. 1999.

[18]Allen, R., Traub, L., Johansen, E. S., Rediniotis, O. K., and Tsao, T., "A MEMS-Based 5-Sensor Probe," AIAA Paper 2000-0252, Jan. 2000.

[19]Johansen, E. S., "Development of a Fast-Response Multi-Hole Probe for Unsteady and Turbulent Flowfields," Ph.D. Dissertation, Aerospace Engineering Dept., Texas A&M Univ., College Station, TX, Dec. 2001.

[20]Siddon, T. E., "On the Response of Pressure Measuring Instrumentation in Unsteady Flow," Univ. of Toronto, Inst. of Aerospace, Rept. 136, Toronto, Jan. 1969.

[21]Fuchs, H. V., "Measurement of Pressure Fluctuations Within Subsonic Turbulent Jets," *Journal of Sound and Vibration*, Vol. 22, No. 3, 1972, pp. 361–378.

[22]Karamcheti, K., *Principles of Ideal-Fluid Aerodynamics*, Wiley, New York, 1966, pp. 278–311.

[23]Kovasznay, L. S. G., Tani, I., Kawamura, M., and Fujita, H., "Instantaneous Pressure Distribution Around a Sphere in Unsteady Flow," Office of Naval Research, Rept. N00014-67-0163-002, Washington, DC, Dec. 1971.

[24]Gossweiler, C. R., Herter, D., and Kupferschmied, P., "Fast Response Aerodynamic Probe Measurements in a Turbulent Pipe Flow," *Proceedings of the 11th Bi-Annual Symposium on Measuring Techniques in Transonic and Supersonic Flows in Cascades and Turbomachines*, Hochschule der Bundeswehr, Munich, 1992.

[25]Gossweiler, C. R., Kupferschmied, P., and Gyarmathy, G., "On Fast-Response Probes: Part 1—Technology, Calibration and Application to Turbomachinery," American Society of Mechanical Engineers, Paper 94-GT-26, June 1994.

[26]Kupferschmied, P., and Gossweiler, C. R., "Calibration, Modeling and Data Evaluation Procedures for Aerodynamic Multihole Pressure Probe Measurements on the Example of a Four Hole Probe," *Proceedings of the 11th Bi-Annual Symposium on Measuring Techniques in Transonic and Supersonic Flows in Cascades and Turbomachines*, Munich, 1992.

[27]Kupferschmied, P., Gossweiler, C. R., and Gyarmathy, G., "Aerodynamic Fast-Response Probe Measurements: State of Development, Limitations and Future Trends," *Proceedings of the 12th Bi-Annual Symposium on Measuring Techniques in Transonic and Supersonic Flows in Cascades and Turbomachines*, Prague, 1994.

[28]Humm, H. J., and Verdegaal, J. I., "Aerodynamic Design Criteria for Fast-Response Probes," *Proceedings of the 11th Bi-Annual Symposium on Measuring Techniques in Transonic and Supersonic Flows in Cascades and Turbomachines*, Hochschule der Bundeswehr, Munich, 1992.

[29]Humm, H. J., Gizzi, W. P., and Gyarmathy, G., "Dynamic Response of Aerodynamic Probes in Fluctuating 3D Flows," *Proceedings of the 12th Bi-Annual Symposium on Measuring Techniques in Transonic and Supersonic Flows in Cascades and Turbomachines*, Prague, 1994.

[30]Humm, H. J., Gossweiler, C. R., and Gyarmathy, G., "On Fast-Response Probes: Part 2—Aerodynamic Probe Design Studies," American Society of Mechanical Engineers, Paper 94-GT-27, June 1994.

[31]Johansen, E. S., and Rediniotis, O. K., "Unsteady Calibration of Fast-Response Pressure Probes, Part 2: Water-Tunnel Experiments," *AIAA Journal*, Vol. 43, No. 4, 2005, pp. 827–834.

[32]Johansen, E. S., and Rediniotis, O. K., "Unsteady Calibration of Fast-Response Pressure Probes, Part 3: Air-Jet Experiments," *AIAA Journal*, Vol. 43, No. 4, 2005, pp. 835–845.

R. Lucht
Associate Editor